Table I. Major Fragments of Four Cyclic Pentapeptides[a]

I, cyclo(D-Phe-Pro-Gly-D-Ala-Pro)

intensity	14	14	7	3	4	5	7	9	100
m/z	469 (M+)	357	286	229	202	153	125	120	70

II, cyclo(Gy-Pro-Gly-D-Ala-Pro)

intensity	10	13	8	3	6	6	100
m/z	379 (M+)	267	196	139	125	112	70

II*, cyclo(Gly-Pro-Gly(^{2}H$_2$)-D-Ala-Pro)

intensity	7	8	5	3	3	5	100
m/z	381 (M+)	269	198	139	125	112	70

III, cyclo(Gly-Pro-D-Phe-D-Ala-Pro)

intensity	14	8	32	8	23	5	12	14	100
m/z	469 (M+)	426	357	343	286	210	139	120	70

IV, cyclo(Ala-Pro-Gly-D-Phe-Pro)

intensity	4	6	3	2	7	3	5	7	6	100
m/z	469 (M+)	357	329	286	210	168	153	125	120	70

[a] Experimental conditions as given in the legend to Figure 1.

Table II. Peptide Bond Torsion Angles

peptide	ω1	ω2	ω3	ω4	ω5	ref
I	180	180	179	179	-158	2c
II	174	-179	177	178	-160	2a
III	171	-177	-173	-176	-158	2d
IV	14	166	-177	175	176	1c

following the Pro$_5$-D-Phe$_1$ bond, specifically at the D-Phe N–C$^\alpha$ bond.

However, comparisons with fragmentation patterns of related peptides demonstrate that the aromatic residue is not essential in directing the ring opening (Table I). The major high mass fragment ions in the EI mass spectrum of II, cyclo(Gly$_1$-Pro$_2$-Gly$_3$-D-Ala$_4$-Pro$_5$), can be accounted for by sequential losses of 112, 71, and 57 or, proline + NH, alanine and glycine, respectively. As above, peaks at the molecular ion minus 43 and 69 suggest that the 112 loss may occur in two steps. An isotopically enriched form of II, cyclo(Gly$_1$-Pro$_2$-Gly$_3$(^{2}H$_2$)-D-Ala$_4$-Pro$_5$), II*, was used to corroborate the assignments of the observed fragment ions. The major high mass ions at m/z 269, 198, and 139 (Table I) are consistent with sequential losses of proline + NH (112), alanine (77), and glycine-d$_2$ (59). These observations suggest that the initial ring opening occurred at the Gly$_1$ N–C$^\alpha$ bond, following the Pro$_5$-Gly$_1$ peptide bond, and that the decomposition mechanism may not require an aromatic side chain. Moreover, inspection of the dihedral angles from crystal structures of peptides I and II reveals that initial cleavage occurs adjacent to the peptide bond that is the *most nonplanar* (Table II).

Fragmentation of a third cyclic pentapeptide, cyclo(Gly$_1$-Pro$_2$-D-Phe$_3$-D-Ala$_4$-Pro$_5$), III (Table I), parallels that observed in I and II. The major high mass ions at 357, 286, and 139 (Table I) are accounted for by sequential losses of proline + NH (112), alanine (71), and phenylalanine (147). These observations suggest that the initial ring opening occurred at the Gly$_1$ N–C$^\alpha$ bond, following the most nonplanar peptide bond in the crystal (Table II).

The analysis of the EI fragmentation pattern of a fourth cyclic pentapeptide, cyclo(Ala$_1$-Pro$_2$-Gly$_3$-D-Phe$_4$-Pro$_5$), IV (Table I), is less straightforward, possibly reflecting more than one ring opening site. Nonetheless, the greatest number of the observed ions can be explained by a ring opening adjacent to the Pro$_2$-Gly$_3$ peptide bond, one of two strongly nonplanar bonds in the crystal (Table II).

It thus appears that a *conformational feature* common to these four peptides influences ring opening: Substantial nonplanarity of a peptide bond correlates with ring cleavage at the following N–C$^\alpha$ bond. We suggest that the neutral and ionized cyclic peptide molecules retain a conformation in the gas phase that is similar to the crystal structure. The bond angle and length distortions associated with a nonplanar peptide bond appear to cause increased

susceptibility to cleavage of proximal bonds in the vibrationally excited ions. Perturbation of the structure is plausible in the cases studied here, as the extents of nonplanarity are large. Theoretical estimates of the energy cost from a peptide bond distortion of 20° are from 5 to 6 kcal/mol.[8] The conformational influences from cyclization appear to be lost once the peptide ring is open, since the fragmentation appears to follow decomposition mechanisms for linear peptides.

(8) Winkler, F. K.; Dunitz, J. D. *J. Mol. Biol.* **1971**, *59*, 169–180.

Measurement of NH–CαH Coupling Constants in Staphylococcal Nuclease by Two-Dimensional NMR and Comparison with X-ray Crystallographic Results

Lewis E. Kay,[†] Bernard Brooks,[‡] Steven W. Sparks,[§] Dennis A. Torchia,[§] and Ad Bax*,[†]

Laboratory of Chemical Physics, NIDDK
Division of Computer Research and Technology
Bone Research Branch, NIDR
National Institutes of Health
Bethesda, Maryland 20892

Structure determination of proteins by NMR relies on measurement of cross relaxation rates (NOE effect)[1] which yields information about interproton distances and on measurements of *J* couplings that are related to dihedral angles through the well-known Karplus equations.[2] As first demonstrated by Marion and Wuthrich,[3] the *J* couplings in small proteins can be measured from the antiphase splittings within a cross peak in phase-sensitive COSY spectra provided that the spectra are recorded with very high resolution in the F$_2$ dimension. However, if the coupling is of the same order or smaller than the ^{1}H line width, measurement of the antiphase splitting can result in a serious overestimate of the actual *J* coupling.[4,5] This problem is particularly severe for

[†] Laboratory of Chemical Physics, NIDDK.
[‡] Division of Computer Research and Technology.
[§] Bone Research Branch, NIDR.
(1) Noggle, J. H.; Schirmer, R. H. *The Nuclear Overhauser Effect, Chemical Applications*; Academic Press: NewYork, 1971.
(2) Karplus, M. *J. Am. Chem. Soc.* **1963**, *85*, 2870–2871.
(3) Marion, D.; Wüthrich, K. *Biochem. Biophys. Res. Commun.* **1983**, *113*, 967–974.
(4) Neuhaus, D.; Wagner, G.; Vasak, M.; Kägi, J. H. R.; Wüthrich, K. *Eur. J. Biochem.* **1985**, *151*, 257–273.

Communications to the Editor

J. Am. Chem. Soc., Vol. 111, No. 14, 1989 5489

the NH protons which experience significant dipolar broadening from the attached nitrogen (^{14}N or ^{15}N) nucleus. Consequently, J couplings between NH and CαH protons are difficult to measure, particularly for proteins larger than about 10 kD which have long rotational correlation times and correspondingly large line widths. Here we present a different approach for measuring NH–CαH J couplings in proteins: By incorporation of ^{15}N in the protein, it is possible to record high sensitivity ^{1}H–^{15}N correlation spectra from which the ^{1}H–^{1}H J couplings can be measured.

As shown recently, to first order the heteronuclear dipolar NH broadening is absent in ^{15}N–^{1}H multiple quantum coherence.[6] This is easily understood by considering the fact that the zero- and double-quantum transition frequencies in a dipolar coupled two-spin system are independent of the size of the dipolar interaction. Hence, the relaxation rate of these transitions does not contain any $J(0)$ heteronuclear dipolar coupling spectral density terms. For macromolecules (in the slow tumbling limit) we find that the relaxation time of multiple quantum ^{15}N–^{1}H coherence can be significantly (15–30%) longer than the transverse relaxation time of the amide proton. The multiple quantum relaxation time determines the F_1 resolution in heteronuclear multiple quantum correlation (HMQC) type spectra.[7-9] Because the NH–CαH J coupling appears in the F_1 dimension of such spectra and because the sensitivity of such spectra for ^{15}N labeled proteins is very high, HMQC spectra are ideally suited for measurement of these couplings.

For the analysis of larger proteins, with very crowded ^{15}N–^{1}H correlation spectra, the most suitable pulse scheme is a variation of the regular HMQC pulse scheme:

$$^{1}\text{H presat}-90_x-\tau-90_\beta-t_1/2-180_\alpha-t_1/2-90_\delta-\tau-(90_\gamma)-\text{acq}(t_2)$$
$$^{15}\text{N} \qquad\qquad\qquad\qquad\qquad\qquad\qquad\qquad\qquad\qquad \text{decouple}$$
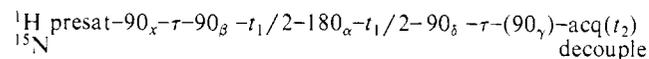
The delay τ is set to 4.5 ms, slightly shorter than $1/(2J_{\text{NH}})$. Data are treated in the standard fashion,[11,12] with data acquired for odd- and even-numbered scans stored separately, the phase cycling is $\alpha = 8(x), 8(y), 8(-x), 8(-y), \beta = x, y, -x, -y, \delta = 32(x), 32(-x), \gamma = 4(y), 4(-y), \text{acq} = 2(x), 2(-x), 2(x), 4(-x), 2(x), 2(-x), 4(x), 2(-x), 2(x), 4(-x), 2(x), 2(-x), 2(x);$ the receiver phase is inverted for the second 32 scans. The 90_γ purge pulse[10] serves to eliminate the dispersive contributions from the line shape that are associated with the J modulation present during the time, t_1. Alternatively, spectra can be recorded without the purge pulse, and slightly higher multiplet resolution can then be obtained; however, in crowded spectral regions the phase twisted line shapes in high-F_1-resolution HMQC spectra cause severe overlap problems. Detailed comparisons of the various different methods will be presented elsewhere.[13]

The measured peak-to-peak doublet splittings in the F_1 dimension are not exactly identical with the J coupling; small differences occur because of partial overlap of the two doublet components (which makes the splitting appear smaller than the J coupling) and because of a small F_1 phase distortion introduced by J modulation during the τ delays (which has the opposite effect), an effect that is not removed by the purge pulse. Analysis of the relatively small differences between measured splitting and actual J coupling for the present experiment and for schemes

(5) Bax, A.; Lerner, L. E. *J. Magn. Reson.* **1988**, *79*, 429–438.

(6) Bax, A.; Kay, L. E.; Sparks, S. W.; Torchia, D. A. *J. Am. Chem. Soc.* **1989**, *111*, 408–409.

(7) Bendall, M. R.; Pegg, D. T.; Doddrell, D. M. *J. Magn. Reson.* **1983**, *52*, 81–117.

(8) Bax, A.; Griffey, R. H.; Hawkins, B. L. *J. Magn. Reson.* **1983**, *55*, 301–315.

(9) Griffey, R. H.; Redfield, A. G. *Q. Rev. Biophys.* **1987**, *19*, 51–82.

(10) Frey, M. H.; Wagner, G.; Vasak, M.; Sørensen, O. W.; Neuhaus, D.; Wörgötter, E.; Kägi, J. H. R.; Ernst, R. R.; Wüthrich, K. *J. Am. Chem. Soc.* **1985**, *107*, 6847–6851.

(11) States, D. J.; Haberkorn, R. A.; Ruben, D. J. *J. Magn. Reson.* **1982**, *48*, 286–292.

(12) Bax, A. *Bull. Magn. Reson.* **1985**, *7*, 167–183.

(13) Kay, L. E.; Bax, A. *J. Magn. Reson.*, in press.

Figure 1. NH doublets of residues V104 (a), A112 (b), and M26 (c) extracted from the ^{15}NH correlation spectra of staphylococcal nuclease complexed with pdTp and Ca^{2+}. Spectra have been recorded (a) with the regular HMQC scheme, by using 30 Hz F_2 line broadening to reduce dispersive components, (b) by processing the same set as phase-modulated data, and (c) by using the pulse scheme that inludes the purge pulse. Exponential line narrowing (5 Hz) in the F_1 dimension was used for all three sections. Spectra have been recorded with (a, b) the regular HMQC pulse scheme without the purge pulse and (c) the scheme with the purge pulse. Sections (a) and (c) are taken parallel to the F_1 axis, and data are processed following the recipe of States et al.[11] Section (b) is taken at an angle of 45° from a spectrum obtained by treating the data as phase-modulated signals.[12,13]
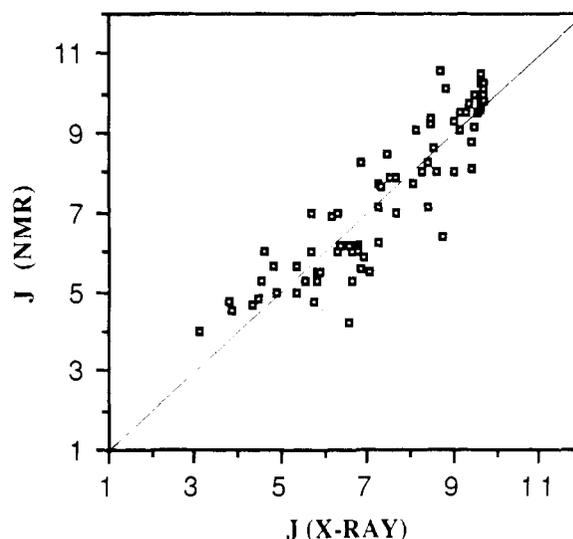

Figure 2. Correlation between J couplings calculated on the basis of the X-ray structure and measured values. The J couplings were calculated from the X-ray structure using the parametrization of the Karplus equation proposed by Pardi et al.[15]

without the purge pulse shows that the required corrections can readily be calculated.[13]

The new approach for measuring J couplings is demonstrated for the protein staphylococcal nuclease, complexed with pdTp and Ca^{2+}, 1.5 mM in 90% H$_2$O, 37 °C, pH 6.5. Data were recorded on a modified NT-500 spectrometer. Figure 1 illustrates three NH doublets, taken from HMQC spectra. All three doublets are resolved, including V104 found in an α-helix, despite the high molecular weight of the complex (18 kD). In total, 75 couplings were measured. Coupling constants were not measurable in cases where NH correlations overlapped, where NH protons exchanged rapidly with solvent, and for 16 NH protons that did not give resolved doublets. For all these unresolved doublets, the X-ray structure predicts $J < 6$ Hz.

Figure 2 shows a correlation between measured J couplings and the values calculated on the basis of the 1.65-Å crystal structure refined with isotropic B factors,[14] showing good agreement and an RMS difference of only 0.84 Hz between the two sets of data. Note that this RMS difference is almost as small as that for the

(14) Lattman, E.; Loll, P. *Proteins: Structure, Function, Genetics*, in press.

BPTI protein, used for the parametrization of the Karplus equation.[15] The RMS difference between measured *J* couplings and the couplings calculated from the crystal structure refined with anisotropic *B* factors was slightly larger, 1.01 Hz. The major contributions to the RMS difference originate primarily from five residues, K70, K78, Y85, E135, and S141. Polar residues K70, Y85, and E135 are involved in intermolecular crystal contacts, K78 is in a sharp turn immediately adjacent to the major inter-protein contact domain in the crystal, and S141 is the last residue observed in the crystal structure.[14]

Energy minimization of the crystal structure or a 100 ps molecular dynamics (MD) simulation of the fully hydrated protein significantly decreased agreement between measured and calculated *J* values. This occurred despite the small RMS deviation (1.50 Å for the backbone atoms, 2.06 Å for all atoms) between the crystal structure and the time averaged MD structure, suggesting that straightforward energy minimization of a good (1.65-Å) crystal structure can lead to false local minima and that 100 ps of dynamics simulation may be insufficient to cure this.

Supplementary Material Available: Table containing the crystal structure ϕ angles of staphylococcal nuclease, complexed with pdTp and Ca^{2+}, the *J* couplings calculated on the basis of these ϕ angles, and the measured *J* couplings (3 pages). Ordering information is given on any current masthead page.

(15) Pardi, A.; Billeter, M.; Wüthrich, K. *J. Mol. Biol.* **1984**, *180*, 741–751.

Ligand-Mediated Reactivity of Niobium–Ketene Complexes

Saul E. Halfon, Maria C. Fermin, and Joseph W. Bruno*

Hall-Atwater Laboratories
Wesleyan University
Middletown, Connecticut 06457

Received December 22, 1988

As part of a study of the chemistry of metal-bound ketenes,[1,2] we sought the preparation of niobocene–ketene complexes so as to extend our earlier work on vanadocene analogues. In the course of these studies, we have used unsymmetrically substituted ketenes to determine reaction stereoselectivities;[3] herein we describe some unprecedented ketene isomerizations as well as a novel synthesis of the first ketene–hydride complex.

Treatment of Cp'_2NbCl ($Cp' = \eta^5$-$C_5H_4SiMe_3$)[4] with ketenes gives rise to the desired ketene complexes (eq 1) in 70–80% yields.

$$Cp'_2NbCl + R^1R^2C{=}C{=}O \rightarrow Cp'_2Nb(Cl)(OCCR^1R^2) \quad (1)$$

1, $R^1 = R^2 = Me$
2, $R^1 = R^2 = Ph$
3, $R^1 = Me; R^2 = Ph$
4, $R^1 = Et; R^2 = Ph$
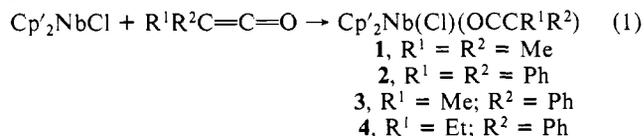
(1) Galante, J. M.; Bruno, J. W.; Hazin, P. N.; Folting, K.; Huffman, J. C. *Organometallics* **1988**, *7*, 1066–1073.

(2) For a review of metal ketene complexes, see: Geoffroy, G. L.; Bassner, S. L. *Adv. Organomet. Chem.* **1988**, *28*, 1–83.

(3) (a) Baigrie, L. M.; Seiklay, H. R.; Tidwell, T. T. *J. Am. Chem. Soc.* **1985**, *107*, 5391–5403. (b) Seikaly, H. R.; Tidwell, T. T. *Tetrahedron* **1986**, *42*, 2587–2613. (c) Haner, R.; Laube, T.; Seebach, D. *J. Am. Chem. Soc.* **1985**, *107*, 5396–5403. (d) Seebach, D.; Amstutz, R.; Laube, T.; Schweizer, W. B.; Dunitz, J. D. *J. Am. Chem. Soc.* **1985**, *107*, 5403–5409.

(4) (a) Hitchcock, P. B.; Lappert, M. F.; Milne, C. R. C. *J. Chem. Soc., Dalton Trans.* **1981**, 180–186. (b) Antinolo, A.; Garcia-Lledo, S.; Marinez de Ilarduya, J.; Otero, A. *J. Organomet. Chem.* **1987**, *335*, 85–90.
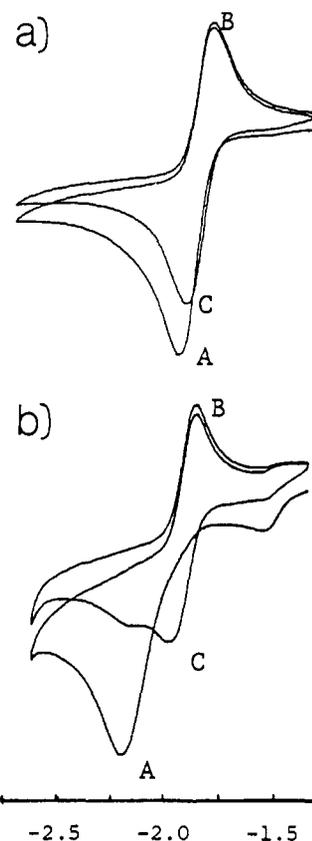

Figure 1. Voltammograms of compounds **2** (a) and **3** (b): 15 mM in THF/1.0 M $Bu_4N^+BF_4^-$. Platinum disk working electrode: potentials are in volts relative to a Ag/Ag^+ reference electrode. Scan rates = 100 mV/s.

This contrasts with Cp_2NbCl, which gives only reductive coupling of two ketene moieties. Although several isomers are possible, the symmetrically substituted ketenes yield only one complex isomer (C=O bound); thus, exo–endo isomerism is not a factor.[5] However, with unsymmetrical ketenes isomeric mixtures *are* observed (via ^1H NMR) due to *E–Z* isomerism about the C=C bond (eq 2).[6] For **3** the *E:Z* ratio is 81:19, while for **4** it is 70:30

exo-*E*   exo-*Z*   (2)
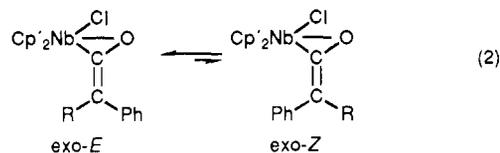
(in C_6D_6); these assignments are based on variable-temperature NMR studies (the *E–Z* equilibrium shifts but remains slow on the NMR time scale up to 75 °C) and an X-ray diffraction study[7] of exo-(*E*)-**4**. Compounds **3** and **4** were allowed to equilibrate (toluene, 20 °C) in the presence of equimolar EtPhC=C=O and MePhC=C=O, respectively. In neither case was ketene exchange observed, so this isomerization constitutes the first example of an intramolecular C=C isomerization of a C=O bound ketene.

Voltammograms for **2** and **3** are presented in Figure 1. The sequential cathodic sweeps exhibit a form commonly associated with an ECEC mechanism (eq 3–5).[8] We suggest that wave A

(5) Alkene ligands normally *do* exhibit *exo–endo* isomerism in $Cp_2Nb(H)$ (alkene) complexes: (a) Klazinga, A. H.; Teuben, J. H. *J. Organomet. Chem.* **1980**, *194*, 309–316. (b) Burger, B. J.; Santarsiero, B. D.; Trimmer, M. S.; Bercaw, J. E. *J. Am. Chem. Soc.* **1988**, *110*, 3134–3146.

(6) Spectroscopic and analytical data are included as Supplementary Material.

(7) Crystal data for **4**: $C_{24}H_{33}NbClOSi_2$, MW = 522.05, monoclinic, $P2_{1/c}$, $a = 7.938$ (5) Å, $b = 15.81$ (2) Å, $c = 21.61$ (1) Å, $\alpha = \beta = 90°$, $\gamma = 95.41$ (6)°, $V = 2700$ (7) Å³, $Z = 4$, $d = 1.28$ g cm⁻³.

(8) (a) Geiger, W. E. *Prog. Inorg. Chem.* **1985**, *13*, 275–352. (b) Kotz, J. C. In *Topics in Organic Electrochemistry*; Fry, A. J., Britton, W. E., Eds.; Plenum: New York, NY, 1986; Chapter 3.